Birefringent coating to remove polarization aberrations

SAWYER MILLER,* D LINAN JIANG, D AND STANLEY PAU

James C. Wyant College of Optical Sciences, University of Arizona, Tucson AZ 85721, USA *samiller@optics.arizona.edu

Abstract: Polarization aberrations are found in most optical components due to a materials-differing response to *s*- and *p*-polarizations. This differing response can manifest either as diattenuation, retardance, or both. Correction of polarization aberrations, such as these, are critical in many applications such as interferometry, polarimetry, display, and high contrast imaging, including astronomy. In this work, compensators based on liquid crystal polymer and anti-reflection thin-films are presented to correct polarization aberrations in both transmission and reflection configurations. Our method is versatile, allowing for good correction in transmission and reflection due to optical components possessing differing diattenuation and retardance dispersions. Through simulation and experimental validation we show two designs, one correcting the polarization aberrations of a dichroic spectral filter over a 170nm wavelength band, and the other correcting the polarization aberration of an aluminum-coated mirror over a 400nm wavelength band and a 55-degree cone of angles. The measured performance of the polarization aberration compensators shows good agreement with theory.

© 2022 Optica Publishing Group under the terms of the Optica Open Access Publishing Agreement

1. Introduction

The interaction of light and thin film depends on numerous properties of both the material and the incident light. Fundamentally, the response is a function of the material's refractive index and the properties of the incident light, such as: wavelength, polarization, and angle of incidence (AOI) [1]. The Fresnel equations give a complete description of the interaction at the thin-film interface, by indicating how much light is transmitted or reflected, as well as the change in phase as a function of polarization [2–4]. Many optical components make use of thin film coatings to enhance the reflection or transmission of the light as well as to realize optical filters where only a band of frequencies is transmitted or reflected [2]. These types of optical filters are commonly used in telecommunications, display, and imaging applications. The designs of the dielectric thin-film coatings are nearly always optimized to maximize the output power of both s- and p-polarizations, allowing for minimal power loss when used at non-normal AOIs. In many of the designs, the optical path differences between the s- and p-polarizations produce a phase shift that changes the polarization state of the outgoing beam [3]. In addition, materials with complex valued refractive indices, such as metals, produce both a phase shift and a polarization-dependent loss at non-normal AOIs as well [1,5]. These interactions manifest as linear retardance and linear diattenuation, causing linearly polarized light to become elliptically polarized, and unpolarized light to become slightly polarized [3,4]. The retardance is dependent on s- and p-polarization components of the incident light, and the amount of phase shift varies as a function of wavelength, AOI, and input polarization state. For many applications, such as polarization sensitive optical systems, polarization aberrations such as these are undesirable and must be controlled [6–12].

In this work, a technique to design and fabricate compensation filters to remove the parasitic retardance and diattenuation is demonstrated. The compensation filters utilize thin-films of birefringent material such as liquid crystal polymer (LCP) to eliminate the parasitic retardance from dichroic optical filters, metal-coated mirrors, and other optical devices such as beamsplitters [3]. We show that a compensation filter for a dichroic optical filter using LCP can operate with a

#458859 Journal © 2022 https://doi.org/10.1364/OE.458859

bandwidth of nearly 170nm, covering the visible spectrum from 460nm to 630nm while keeping the parasitic retardance to no more than 10 degrees. We design and fabricate a compensator to control the polarization aberrations from a commercial dichroic filter (Edmund Optics, Model 69-205), which has a parasitic retardance measured to exceed a quarter wave at 600nm [13,14]. In addition, we design and fabricate a polarization compensator to control retardance and diattenuation for an aluminum coated mirror [6–8,15].

2. Theory

Two common optical components generating polarization aberrations are studied in this work. The first is a dichroic optical filter, a type of multi-layer interference filter. Dichroic filters are typically used to filter incident light into two raypaths, each with different wavelength bands. We design a compensator to correct for the parasitic retardance generated by this kind of filter. The second design is for an aluminum mirror. We design a compensator to reduce both the retardance and diattenuation in such a mirror. Our technique can be generalized to other types of interference filters and metal coatings.

2.1. Phase shift from dichroic filters

Many dichroic filters are constructed of alternating layers of thin-films. Interference between multiple ray-paths is introduced, allowing for certain wavelength regions to transmit or be reflected. These filters can be designed for normal AOI, as well as non-normal AOI. Of interest are the filters which are designed for non-normal AOIs [14]. Filters such as these are optimized to have low linear diattenuation; i.e. *s*- and *p*-polarizations transmit with the same power. However, due to the interference and different optical path length (OPL) for *s*- and *p*-polarizations, linear retardance is produced, causing the polarization state of the light to change. For polarization sensitive optical systems, the parasitic retardance introduced by the OPL difference can be quite severe. For example, a commercial dichroic filter (Edmund Optics, Model 69-205), was measured to have over a quarter wave retardance at 600nm [13].

We analyze the polarization effects of the dichroic filter using the Mueller-Stokes calculus. The Mueller-Stokes calculus is used rather than the Jones calculus in this situation given the intended use of the dichroic filter. The dichroic filter used in this study is designed to operate as a shortpass filter, transmitting in the range of 450nm to 650nm. Mueller-Stokes analysis is applicable to broadband light, as the dichroic filter is normally used with polychromatic incoherent light, rather than monochromatic coherent light where Jones calculus would be more appropriate [3].

In Fig. 1(a), an ideal, non-polarizing Mueller matrix as a function of wavelength is shown. This matrix is an identity matrix for all wavelengths, meaning all polarization states input will retain their Stokes parameters. For dichroic filters, non-polarizing behavior in the operating regime is desired. Figure 1(b) shows the measured Mueller matrix of the dichroic filter at the designed 45-degree AOI, using an Axometrics AxoScan Mueller matrix polarimeter. As shown in the measured Mueller matrix, the diattenuation is non-existent, following the intended design. However, a large amount of retardance is found in the 3x3 retarder sub-matrix. The measured retardance is also non-uniform as a function of wavelength, showing dispersive behavior.

To compensate for the parasitic retardance, multiple layers of birefringent material are used. In this work, nematic phase liquid crystal polymer (LCP) is used as the birefringent thin-films. In an attempt to find compensator designs that best correct the parasitic retardance, materials with different dispersion are considered [16]. Figure 2 shows retardance as a function of wavelength for two commercially available LCPs, RMM141C and RMM1707 (EMD Electronics, the Electronics business of Merck KGaA, Darmstadt, Germany). Both materials are prepared in the exact same manner; however, RMM1707 has a much higher linear birefringence and more birefringence dispersion over the wavelengths of 400nm-800nm as compared to RMM141C. Both materials are A-plate LCPs (i.e., the *c*-axis is in the same plane as the substrate) [17].

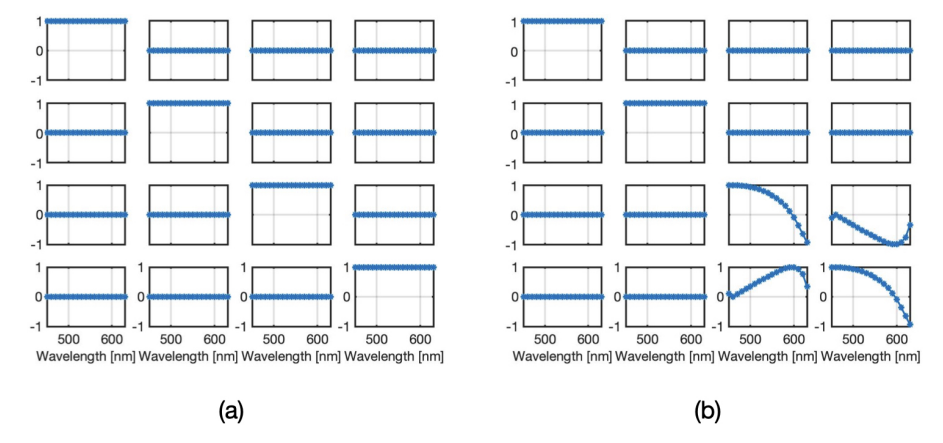


Fig. 1. (a) Perfect non-polarizing optics have a Mueller matrix represented by the identity matrix. No polarization change occurs since the Stokes parameters remain unchanged after interaction. (b) The measured Mueller matrix as a function of wavelength for a dichroic filter with polarization aberration is shown. Due to the interference in the dielectric film stack, *s*- and *p*-polarizations have an unequal optical path length causing a linear retardance. In this example, the parasitic linear retardance is non-uniform as a function of wavelength.

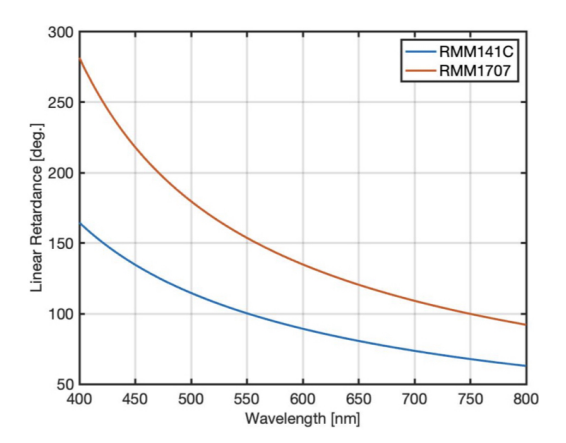


Fig. 2. The plot shows the linear retardance of thin film samples of RMM141C and RMM1707 in the wavelength range of 400nm-800nm. Both samples are prepared in the exact same manner and are defined to have a retardance thickness (Ct) of 1.

With two different types of materials and the measured Mueller matrix of the dichroic, it is now possible to setup a merit function to solve for the parameters of the compensator itself. Each layer of the compensator has three variables: (1) the material, (2) the fast-axis direction, and (3) the thickness of the material. Figure 3 shows how the compensator is constructed from multiple layers of nematic LCP, each with a different physical thickness, d, and fast-axis angle, θ . Each layer can have a different model of nematic LCP as well, allowing for materials with different dispersion characteristics to be used together.



Fig. 3. The polarization aberration compensator is fabricated from multiple layers of nematic phase A-plate liquid crystal polymer. Each layer has a different fast-axis orientation and physical thickness, both of which are determined using the optimization routine. Each layer can also use a different material as well, such as RMM141C or RMM1707.

Numerous designs exist, especially when additional layers are added and there is freedom to choose the material for each layer. In this work, we have limited ourselves to 4-layer designs utilizing commercially available LCP materials, where the performance is quite good, although our method can be generalized to larger number of layers and other materials. The level of correction will continue to increase as the number of layers increases. The Mueller matrix of an *n*-layered compensator and dichroic filter can be defined as:

$$M = L_n \cdots L_3 L_2 L_1 D \tag{1}$$

where M is the cumulative Mueller matrix of the compensator and dichroic filter, L_i are the Mueller matrices of the individual layers of the compensator, and D is the Mueller matrix of the dichroic filter. Each L_i is a function of θ , the fast-axis orientation and δ , the linear retardance of the LCP. To properly model the birefringence dispersion of the LCP, the single-band dispersion model is used [18].

$$\Delta n(\lambda) = G \frac{\lambda^2 \lambda^{*2}}{\lambda^2 - \lambda^{*2}} \tag{2}$$

G is a proportionality constant, approximately linearly proportional to the physical film thicknesss, d. λ^* is the resonant wavelength of the material, and λ is the wavelength of interest. Relating the modeled birefringence dispersion to the retardance is shown below for an A-plate.

$$\delta(\lambda) = \frac{2\pi}{\lambda} \Delta n(\lambda) d = Ct \frac{\lambda^2 \lambda^{*2}}{\lambda^2 - \lambda^{*2}}$$
 (3)

C is a dimensionless scalar; t is the retardance thickness of the LCP. Standard samples of each material are made, and Ct and λ^* are fit based on the measured Mueller matrices using an Axometrics AxoScan Mueller matrix polarimeter. Using the fits for Ct and λ^* , other samples with different physical thicknesses from the standards, d, can be simulated. For simplicity, the standard samples plot in Fig. 2 have a retardance thickness set to be equal to 1. All fitted layers have thicknesses which refer to these standard samples.

With the 4-layer design and the measured Mueller matrix of the dichroic filter, a merit function can be defined.

$$\nu_{\lambda} = \sum_{i=0}^{3} \sum_{j=0}^{3} (M_{ij}(\lambda) - I_{ij})^{2}$$
(4)

Here, M is the cumulative Mueller matrix of the compensator and dichroic filter, and I is the ideal, non-polarizing, identity matrix. Each of the components of the two Mueller matrices are compared and combined to a single scalar value. This allows for a constrained non-linear multi-variable solver to be used in the minimization of ν_{λ} . Dispersion data is taken into account from Eq. (3) during minimization of Eq. (4). Additionally, is should be noted that the merit function defined in Eq. (4) is only designed to have high success finding compesenator Mueller matrices made from non-absorbing materials.

2.2. Normal angle of incidence design: Dichroic filter

Given the design of the commercial dichroic filter shown in Fig. 1(b), two different configurations exist as it is optimized for a 45-degree AOI. In the first configuration to be discussed, the compensator is on a separate substrate, and the light will be normally incident. Figure 4 shows an outline of the basic optical system and how the compensator is integrated.

Having the phase shift compensator at a normal AOI simplifies the design, since the retardance of each component layer can be represented by Eq. (5)

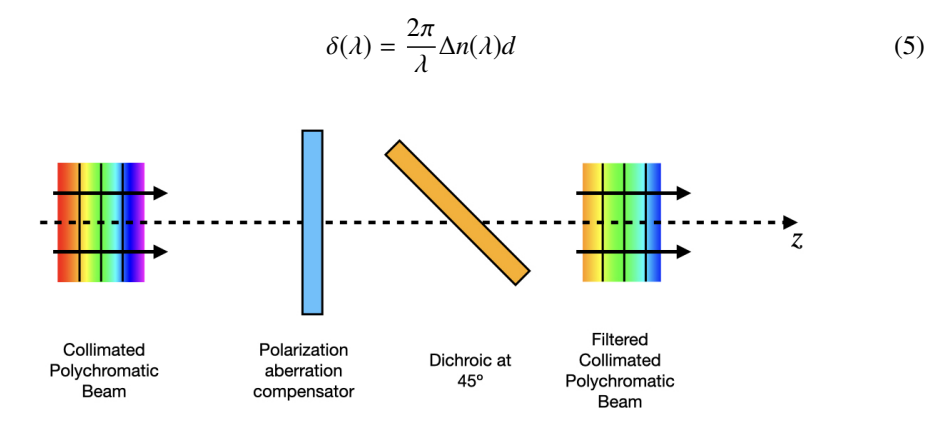


Fig. 4. Schematic of the optical system showing the position of the phase shift compensator, designed to operate at normal incidence, and the dichroic filter operating at 45 degrees.

The phase shift compensator can also be placed anywhere in the optical system as long as the light is normally incident and m is properly calculated in Eqs. (1) and (4). Equations (1)–(5) were used in the optimization of a compensator for normally incident light as shown in Fig. 4. The angle and thickness for each of the four layers for the global optimum is calculated using the MATLAB Global Optimization Toolbox and the non-linear multivariable solver, fmincon. The corrected Mueller matrix and residual retardance is plot in Fig. 5. Figure 5(a) shows good correction in the wavelength range of 450nm to 630nm, nearly the entire bandwidth of the dichroic filter, as the Mueller matrix is close to identity as a function of wavelength. Figure 5(b) shows the calculated retardance. The compensator does an excellent job of removing nearly all of the residual retardance from the dichroic. The original parasitic retardance from the uncorrected dichroic filter is plotted for comparison.

The parameters of the compensator are shown below in Table 1. It should be noted that the fast-axis alignment is in reference to the *s*- and *p*-polarizations incident to the dichroic filter. For this design, a fast-axis orientation of 0 degrees corresponds to the *s*-polarization state for the

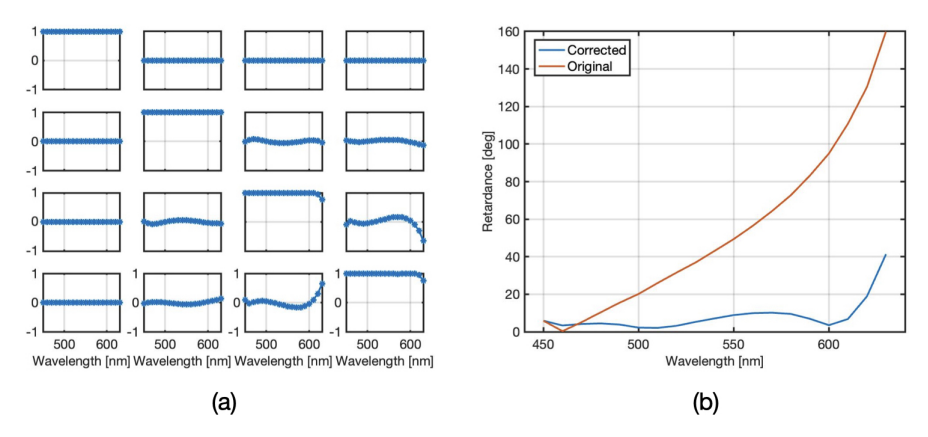


Fig. 5. (a) Plot of the simulated Mueller matrix of the combined polarization aberration compensator and the short-pass dichroic filter. (b) Residual retardance from the combination of the compensator and short pass dichroic filter is plotted in blue. The proposed optical system shows nearly perfect correction from 450nm to 630nm, as residual retardance is kept below 10 degrees. The measured retardance from the dichroic filter only is plotted in orange for comparison.

dichroic filter and a fast-axis orientation of 90 degrees corresponds to the *p*-polarization state for the dichroic filter.

Table 1. Parameters of the normal AOI design are shown. The retardance thickness is in reference to the standard samples plotted in Fig. 2, which have a retardance thickness of 1.

Layer	Material	Fast-axis Alignment	Retardance Thickness (Ct)
1	RMM1707	25.7	1.59
2	RMM1707	87.5	1.77
3	RMM1707	152.4	1.72
4	RMM141C	19.8	0.25

2.3. Non-normal angle of incidence design: dichroic filter

The second configuration studied is the non-normal AOI design. In this design, the compensator is placed at the same AOI as the dichroic filter: in this case, 45-degrees. This type of design has the significant advantage of placing dichroic filter and compensator on the same substrate, allowing for a small form factor. Figure 6 shows a schematic of the optical system, with the phase compensator at a 45-degree AOI, the same angle as the dichroic filter.

Having the phase compensator to operate at non-normal AOI introduces a more complex calculation of the retardance of each layer. The retardance of each layer can be calculated as a function of wavelength (λ) , physical film thickness (d), extraordinary index of refraction (n_e) , ordinary index of refraction (n_o) , fast-axis orientation (ϕ_n) , and the elevation and azimuth AOIs $(\theta_0 \text{ and } \phi_0)$ [17].

$$\delta(\lambda) = \frac{2\pi}{\lambda} d \left[n_e \sqrt{1 - \frac{\sin^2 \theta_0 \sin^2(\phi_n - \phi_o)}{n_e^2} - \frac{\sin^2 \theta_0 \cos^2(\phi_n - \phi_o)}{n_o^2}} - n_o \sqrt{1 - \frac{\sin^2 \theta_0}{n_o^2}} \right]$$
(6)

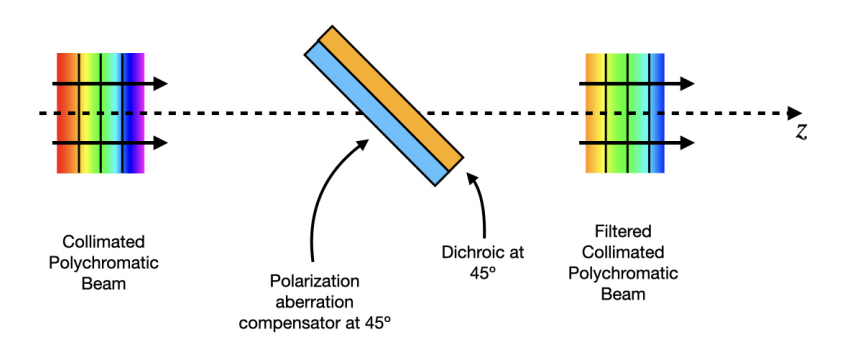


Fig. 6. Schematic of the optical system showing the position of the phase shift compensator, designed to operate at a 45-degree angle of incidence, the same as the dichroic.

Plotting Eq. (6) as a function of θ_0 and ϕ_0 shows a saddle with astigmatic behavior. To properly account for dispersion, Eq. (3) is modified slightly to account for the astigmatic behavior.

$$\delta(\lambda) = Ct \frac{\lambda^2 \lambda^{*2}}{\lambda^2 - \lambda^{*2}} + a\sin(\theta_0)\cos(2\phi_0)$$
 (7)

Here a is a fitting parameter and $\sin(\theta_0)\cos(2\phi_0)$ is a functional representation of the saddle behavior demonstrated by A-plates given the c-axis is parallel to the plane of the substrate and polar coordinates for the incident light are used. Measurements of the standard LCP samples in Fig. 2 are taken as a function of wavelength and polar angles (θ_0 and ϕ_0) using an Axometrics AxoScan Mueller matrix polarimeter. Utilizing Eq. (7) into the merit function in Eq. (4), we can calculate the parameters of an optimized design, as shown in Fig. 7.

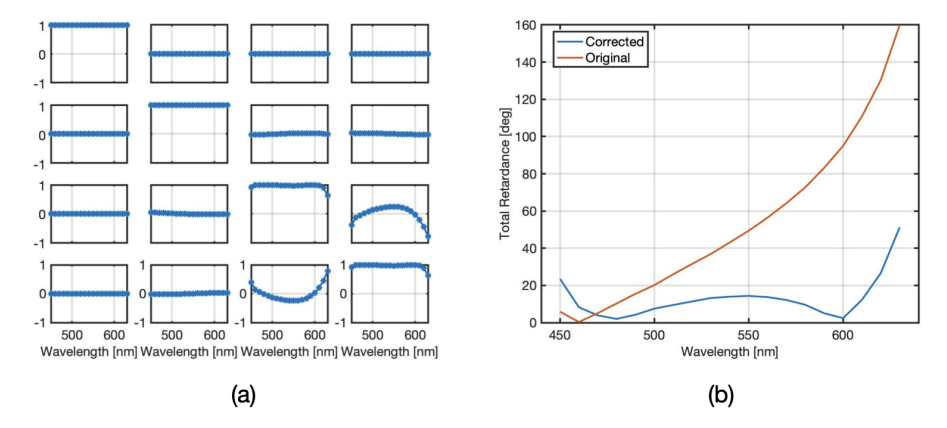


Fig. 7. (a) Plot shows the simulated Mueller matrix of the combined polarization aberration compensator and short-pass dichroic filter, both at a 45-degree angle of incidence. (b) Residual retardance from the combination compensator and short-pass filter is plotted in blue. The proposed optical system shows nearly perfect correction from 450nm to 610nm, as residual retardance is kept below 10 degrees. The measured retardance from the dichroic filter only is plotted in orange for comparison.

Figure 7(a) shows the simulated Mueller matrix of the corrected dichroic filter when operating at a 45-degree AOI. The correction is quite good and produces near-identity matrix behavior from 450nm to 610nm. Additionally, Fig. 7(b) shows the remaining parasitic retardance in blue and the original retardance from the dichroic filter in orange, demonstrating a significant improvement in polarization aberration reduction. The parameters of the 45-degree AOI design are shown

below in Table 2. Material, retardance thickness, and fast-axis alignment are all specified. As the normal AOI design in the previous section, a 0-degree fast-axis alignment corresponds to the *s*-polarization state of the combined tilted compensator and dichroic filter. The *p*-polarization state corresponds to a fast-axis alignment of 90 degrees.

Table 2. Parameters of the 45 degree AOI design are shown. The retardance thickness is in reference to the standard samples in Fig. 2, which have a retardance thickness of 1.

Layer	Material	Fast-axis Alignment	Retardance Thickness (Ct)
1	RMM141C	1.3	2.06
2	RMM141C	151.8	0.98
3	RMM141C	37.3	1.38
4	RMM1707	150.4	0.63

2.4. Compensator design for reflection: aluminum coated mirror

Other common interfaces suffering from parasitic retardance are reflections from metals at non-normal AOIs. In interfaces such as these, the imaginary component in the index of refraction causes a phase shift for both s- and p-polarizations, as well as linear diattenuation [3,6–8,15,19]. Additionally, small optical path differences occur due to the thin-films of oxides which naturally occur when metals are exposed to oxygen. The same concept of a polarization aberration compensator can be applied in this application as well.

The polarization aberration compensator consists of two components: a LCP layer to correct for the retardance and an anti-reflection (AR) coating to correct for the diattenution [20]. In order to accurately design the device, the Jones calculus is used to properly account for interference and differing phases for the calculated wavelengths. Additionally, to preserve a small form factor, the polarization aberration compensator is designed to be coated directly onto the aluminum or onto a separate substrate which lies parallel to the aluminum surface. This causes the phase compensator to be placed in a double-pass configuration, as shown in Fig. 8. The design is also desired to be free of azimuthal constraints, allowing for any combination of *s*- and *p*-polarizations to be corrected [21]. The Jones matrix describing a Fresnel transmission or reflection is described as

$$J_{sp} = \begin{bmatrix} x_s & 0\\ 0 & x_p \end{bmatrix} \tag{8}$$

where x_s and x_p are the Fresnel transmission or reflection coefficients for s- and p-polarizations, respectively. An ideal Jones matrix for reflection is calculated as

$$r = \begin{bmatrix} 1 & 0 \\ 0 & -1 \end{bmatrix} \tag{9}$$

Ideally, the Jones matrix of a mirror is equal to *r* over a band of wavelengths; however due to dispersion of materials, both the diattenuation and retardance vary as a function of wavelength. Additionally, the Fresnel equations are dependent on AOI, thereby causing variation in the polarization aberrations as well.

Given this configuration, the cumulative Jones matrix for the system is calculated as

$$J = F_2 \cdot C \cdot A \cdot C \cdot F_1 \tag{10}$$

where F_1 and F_2 are the Jones matrices for AR coating, C is the Jones matrix of the negative C-plate, and A is the Jones matrix describing reflection from aluminum. Using singular value

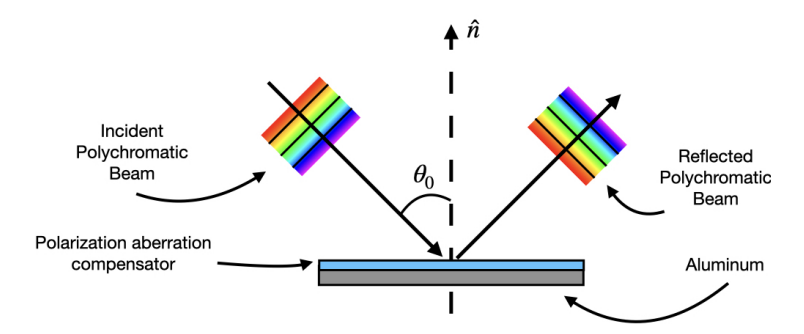


Fig. 8. Schematic of the optical system is shown, illustrates the position of the polarization aberration compensator designed to operate at a range of AOIs. The phase compensator is placed in a double-pass configuration.

decomposition of J, diattenuation and retardance can be calculated as a function of wavelength and AOI. Given that all components in J contribute diattenuation and retardance individually, the system must be optimized as a product for accurate correction. The merit function for optimization reflects this as

$$\nu_{\lambda,\theta_0} = \sum_{\lambda=400 \text{nm}}^{800 \text{nm}} \sum_{\theta_0=0 \text{deg}}^{55 \text{deg}} \sqrt{d(\lambda,\theta_0)^2 + (180 - \phi(\lambda,\theta_0))^2}$$
 (11)

where d is the diattenuation of J, and ϕ is the retardance of J. As we would like to solve the polarization aberrations resulting from the parasitic retardance over a large cone of angles, A-plate materials are not best suited for the application. As described in Eq. (6), A-plates have an azimuthal dependency at non-normal AOIs. To remove the dependency, a C-plate material can be used as the phase compensator instead. The retardance (δ) for a C-plate can be described as [17]

$$\delta(\lambda) = \frac{2\pi}{\lambda} n_o d \left[\sqrt{1 - \frac{\sin^2 \theta_0}{n_e^2}} - \sqrt{1 - \frac{\sin^2 \theta_0}{n_o^2}} \right]$$
 (12)

With the C-plate configuration, the azimuthal dependency on the waveplate is removed as the c-axis of the material is perpendicular to the plane of the substrate. The retardance is now only a function of AOI, θ_0 , the physical thickness, d, the wavelength, λ , and the extraordinary and ordinary indices of refraction, n_e and n_o . To account for the dispersion as well as the angle of incidence dependency, Eq. (3) is modified as the following:

$$\delta(\lambda) = Ct \frac{\lambda^2 \lambda^{*2}}{\lambda^2 - \lambda^{*2}} \sin^2(\theta_0)$$
 (13)

While the C-plate can eliminate any azimuthal dependence on the compensation, the correct type of C-plate needs to be selected. Common C-plates are classified as positive, where the extraordinary index of refraction is larger than the ordinary index of refraction. Such a property causes the s-polarization state to be the fast eigenpolarization, making the correction for aluminum more difficult. The suitable choice utilizes a negative C-plate material, where the extraordinary index of refraction is less than the ordinary index of refraction. The p-polarization state is now the fast eigenpolarization, making the correction for aluminum possible. Equation (11) is minimized using the MATLAB Global Optimization Toolbox and the nonlinear multivariable solver, fmincon. The solver determines the thickness of the negative C-plate layer using the dispersion data from LCP model RMM1082 (commercially available from EMD Electronics).

Additionally, the AR coating thickness is determined using dispersion data from a low index amorphous fluoropolymer, Teflon AF1601 (commercially available from DuPont de Nemours, Inc.) [22].

For comparison with fabricated devices, it is useful to convert Eq. (9) to a Mueller matrix. The Mueller matrix for ideal reflection is shown below in Eq. (14).

$$R = \begin{bmatrix} 1 & 0 & 0 & 0 \\ 0 & 1 & 0 & 0 \\ 0 & 0 & -1 & 0 \\ 0 & 0 & 0 & -1 \end{bmatrix} \tag{14}$$

Figure 9(a) describes the ideal Mueller matrix for reflection as a function of wavelength. This is the same matrix shown in Eq. (14). With the polarization aberration compensator, we would like the Mueller matrix for all AOIs to be as close to the one represented in Fig. 9(a). Figure 9(b) shows simulations of the polarization aberrations present due to reflection from aluminum at various AOIs. As the AOI increases, so does the retardance. Matrix elements $m_{0,1}$ and $m_{1,0}$, outlined with dashed boxes, are plotted with a reduced scale to show detail of the small amounts of linear diattenuation generated.

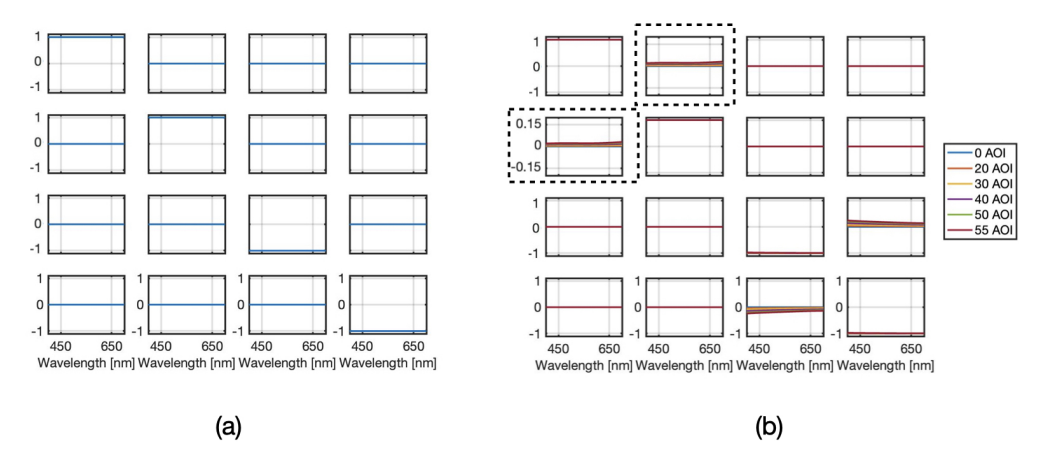


Fig. 9. (a) Ideal Mueller matrix for reflection as a function of wavelength is shown. This matrix is used in the figure of merit, described in Eq. (14). (b) The simulated Mueller matrices as a function of wavelength for different AOI for an aluminum coated mirror are shown. Increasing the AOI increases the linear retardance. Elements $m_{0,1}$ and $m_{1,0}$ are outlined with dashed boxes and plotted with reduced scale to show detail.

Figure 10(a) shows simulations of aluminum with negative C-plate material coated on top at various AOIs. The Fresnel reflections at the air/negative C-plate interface are calculated as a function of the extraordinary and ordinary indices of refraction as well as the AOI. The birefringence of the negative C-plate material used is approximately 0.04. The ordinary index of refraction is 1.5, thereby setting the extraordinary index of refraction to be 1.46. The linear retardance produced by the aluminum is well corrected at all AOIs and wavelengths using the negative C-plate material. However, the linear diattenuation increases as a function of AOI. As the AOI increases, the amount of linear diattenuation at the air/negative C-plate interface and negative C-plate/aluminum interface increases due to the difference in Fresnel reflections for s- and p-polarized light. Matrix elements $m_{0,1}$ and $m_{1,0}$, outlined in dashed boxes, are plotted with reduced scale to show detail of the diattenuation. Figure 10(b) shows the corrected Mueller

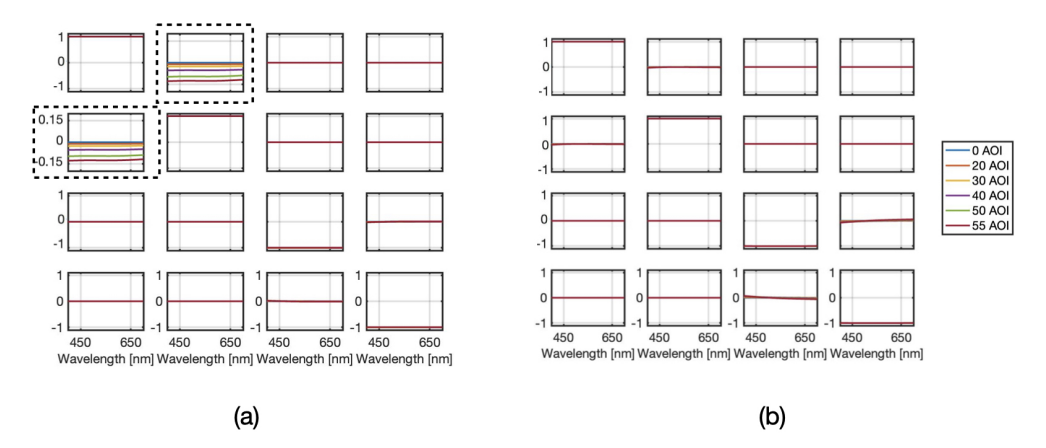


Fig. 10. (a) The Mueller matrix of an aluminum coated mirror with a negative C-plate coating is shown as a function of wavelength, illustrating the retardance correction of the negative C-plate. The negative C-plate introduces additional diattenuation; elements $m_{0,1}$ and $m_{1,0}$ are plotted with reduced scale to show detail. (b) The Mueller matrix of an aluminum coated mirror with both a uniaxial C-plate and an AR coating is shown as a function of wavelength. Our results show a correction with a bandwidth of 400nm over a 55-degree cone of angles.

matrix for aluminum with a single negative C-plate layer and AR coating. The AR coating eliminates the linear diattenuation introduced by the aluminum reflection and reflections from the air/negative C-plate interface. It is noted that both the thickness of the negative C-plate and AR coating are optimized together to ensure that the polarization aberrations are minimized. This design can correct both the diattenuation and retardance of the aluminum coated mirror, reducing the polarization aberrations up to a ± 55 -degree cone. Furthermore, Fig. 11 details additional metrics concerning the correction of reflection from aluminum.

Figure 11(a) shows the reduction in diattenuation resulting from our method of negative C-plate and AR coating. The diattenuation is kept below 5% across a 400nm band up to a 55 degree cone of angles. Figure 11(b) plots the reduction in diattenuation for the various AOIs, with up to a 100% reduction in diattenuation. Figure 11(c) plots the reflectance for the complete layer stack showing improved performance due to the AR coating as well. Finally, in Fig. 11(d), the reduction in retardance due to the negative C-plate is plotted. The residual retardance is also kept below 5 degrees for the entire 400nm band up to a 55 degree cone of angles.

The method described here is effective not only for aluminum; it can also be applied to compensation of other metal coated mirrors. Table 3 details the thicknesses of the negative C-plate and AR coating for aluminum, silver, and gold.

Additionally, it should be noted that the diattenuation due to reflection from metal as well as the air/C-plate interface can be corrected using a C-plate layer and dichroic dye combination, utilizing the guest-host interaction [23]. Using the dichroic dye shows potential for a wider wavelength bandwidth in operation. However, a non-polarization-dependent transmission loss is introduced with the usage of dichroic dyes.

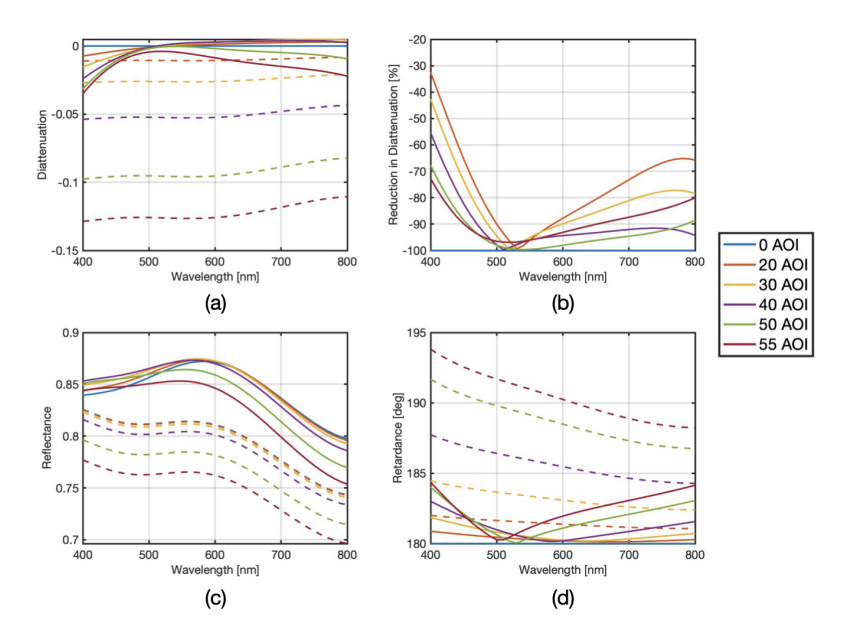


Fig. 11. A comparison of the aluminum coated mirror and aluminum coated mirror with negative C-plate and AR coating is shown. Original uncorrected values are presented with dashes lines, while corrected values are plotted with solid lines. (a) Plot shows improvement of diattenuation across a 400nm band in the visible spectrum. (b) Plot shows reduction in diattenuation for various AOI, with up to a 100% reduction. (c) Reflectance of the aluminum coated mirror is shown as a function of wavelength. Using the AR coating reduces absorption and unwanted reflections from the negative C-plate layer. (d) Plot shows the resulting retardance curves, corrected by the negative C-plate layer. Up to a 55-degree cone of angles is corrected across a 400nm band to less than 5 degrees of retardance.

Table 3. Optimized thickness parameters for reflections with minimized polarization aberrations from aluminum, silver, and gold.

Metal	LCP Thickness (Ct)	AR Coating Thickness (nm)
Aluminum	0.198	130
Silver	0.333	130
Gold	0.405	210

3. Experimental methods and materials

3.1. Materials and characterization

Wafers of a 1.5-inch diameter and 500 μm thickness used in this work are made from polished soda lime glass, selected for its excellent optical transmission in the visible spectrum and non-polarizing behavior (Valley Design Corp. Shirley, MA, USA). Before fabrication, each wafer is cleaned and prepared using oxygen plasma treatment. Three different types of LCP are used in the work. The two nematic A-plate materials are models RMM141C and RMM1707. The negative C-plate material is model RMM1082. All materials are commercially available (EMD Performance Materials, a unit of Merck KGaA, Darmstadt, Germany). The A-plate materials are dissolved in toluene, while the negative C-plate material is dissolved in propylene glycol monomethyl ether acetate (PGMEA) to allow for spincoating application. The photoalignment layer consists of SD1 dissolved in N,N dimethylformamide (DMF) [24]. Polarization measurements are carried out using an Axometrics AxoScan Mueller matrix polarimeter (Axometrics, Hunstville, AL, USA). Metal-coated mirror samples used the in study were prepared by evaporating aluminum onto a highly polished silicon wafer to obtain a 50nm-thick coating film using a Temescal FC2500 E-beam Evaporator (Ferrotec USA, Santa Clara, CA, USA).

3.2. Fabrication of dichroic compensator

The normal AOI design for a dichroic compensator presented in Section 2.2 is fabricated. This design uses only A-plate materials.

- 1 The substrate is cleaned using oxygen plasma for 1 minute.
- 2 SD1 dissolved in DMF at a 0.38% weight concentration is dispensed through a $0.2\mu m$ PTFE filter and spin-coated onto the substrate at 3000 RPM for 30 seconds. The wafer is then baked on a hot plate at 150°C for 5 minutes.
- 3 The SD1 is then aligned using a UV dichroic polarizer (Boulder Vision Optik, Boulder, CO, USA) and a 365nm UV light source with 150mJ/cm² energy for 5 minutes.
- 4 Either RMM141C or RMM1707 is dispensed through a 0.2μm PTFE filter and spin-coated onto the aligned SD1 layer. Spin speed varies given the desired thickness of the layer. RMM141C rests on the substrate at room temperature for 1 minute post spin-coating, whereas RMM1707 is baked on a hot plate at 55°C for 1 minute post spin-coating.
- 5 The LCP material is then cured under nitrogen atmosphere for 5 minutes using the 365nm light source with 150mJ/cm² energy.
- 6 Additional layers can now be added, either using additional substrates or by depositing a layer of SiO₂ and repeating Steps 2-5 again.

3.3. Fabrication of aluminum compensator

The aluminum compensator design presented in Section 2.4 is fabricated. This design uses only negative C-plate material. Only the liquid crystal layer is applied in this fabrication, no AR coating is applied.

- 1 The substrate is cleaned using oxygen plasma for 1 minute.
- 2 RMM1082 is dispensed through a $0.2\mu m$ PTFE filter and spin-coated onto the cleaned wafer at 3000 RPM for 1 minute. The wafer is then baked on a hot plate at 70°C for 1 minute post spin-coating.
- 3 The LCP material is then cured under nitrogen atmosphere for 5 minutes using the 365nm light source with 150mJ/cm² energy.

4. Results

A compensator utilizing A-plate material as described in Section 2.2 is fabricated and tested. For better control and ease of fabrication, the different layers are fabricated on separate substrates, subsequently aligned, and then combined to form the compensator. The layers can, in principle, be fabricated on the same substrate with a barrier layer between any two adjacent layers, or with thin intermediate twisting layers [25,26]. Our design utilizes two thick RMM1707 layers, one thinner RMM1707 and one thinner RMM141C layer. The two thick layers are fabricated first, and retardance is measured. A second optimization is carried out to determine the parameters of the remaining two layers using the measured parameters of the first two fabricated thick layers as constraints. The two remaining layers are subsequently fabricated. The dual optimization improves the final performance of the compensator, since we do not have exact control in coating of the thick LCP layer. The final design is presented in Table 4.

Table 4. Re-optimized values for the normal AOI design presented in Section 2.2. The retardance thickness is in reference to the standard samples plot in Fig. 2, which have a thickness of 1.

Layer	Material	Fast-axis Alignment	Retardance Thickness (Ct)	
1	RMM1707	156.3	1.82	
2	RMM1707	82.8	1.86	
3	RMM1707	16.3	1.25	
4	RMM141C	14.6	0.90	

The final design shows nearly identical performance in the wavelength region of 460nm to 600nm compared to the design in Section 2.2, showing approximately 20 to 30nm of bandwidth loss due to the change in layer thickness.

Each of the substrates are aligned appropriately in the stack and oriented properly based on measurements using the Axometrics polarimeter. Measurement of the Mueller matrix of the combined stack is presented in Fig. 12(a) and compared with the simulated design.

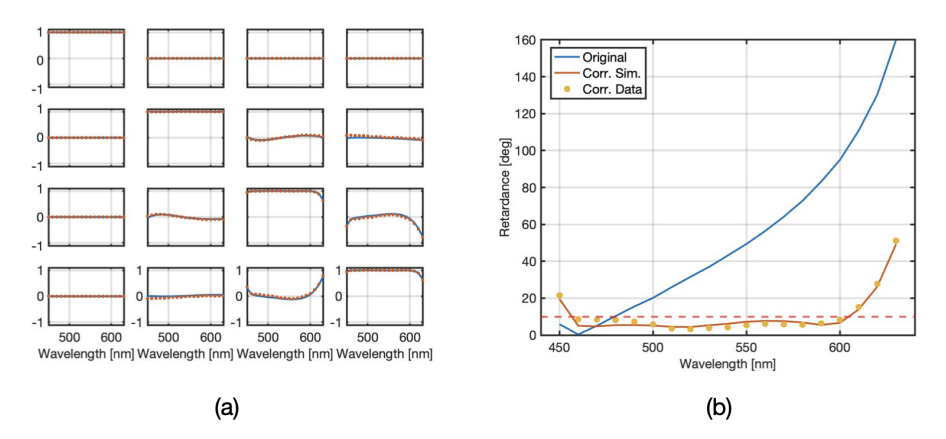


Fig. 12. (a) Mueller matrix of the design (solid lines) and measured data (dots) is shown. The fabricated device shows excellent agreement with theory. (b) The residual retardance for the design and measured data are compared for the compensated and uncompensated dichroic filter. The red dashed line represents 10 degrees of retardance. The compensated design has less than 10 degrees of residual retardance from 460nm to 600nm, while the dichroic filter alone has retardance that monotonically increases.

Figure 12(b) shows the residual retardance present in the measured device as compared with theory and an uncorrected dichroic. The fabricated device keeps the residual retardance below 10 degrees in the wavelength region of 460nm to 600nm, which is well below the retardance of the dichroic filter alone. Using the Lu-Chipman decomposition [27], measured Mueller matrices were decomposed into their respective retarder, diattenuator, and depolarization components. The thicker RMM1707 layers presented 3 to 5% depolarization. This is attributed to slight crystallization of the older RMM1707 material which leads to an overall 8 to 10% undesired depolarization in the device. The depolarization is not an inherent limitation of the material, and we believe the crystallization may be caused by the age of the RMM1707 (approximately four years old).

A compensator utilizing negative C-plate material as described in Section 2.4 is also fabricated and tested to demonstrate the flexibility of our method. A 50nm thick layer of aluminum was evaporated onto a highly polished silicon substrate and served as a metal-coated mirror. For demonstration purposes, only the negative C-plate layer was fabricated. No AR coating was added to this fabricated compensator, thereby leaving the diattenaution uncorrected. The fabricated compensator was then placed on top of the mirror. The combined layer were measured using the Axometrics polarimeter. The Mueller matrix measurements are plotted in Fig. 13(a). The retardance is well corrected by the negative C-plate, as shown by the 3x3 sub-matrix. The diattenuation is uncorrected, as shown by the analyzer vector, as expected. The magnitude and sign of the diattenuation match the uncorrected simulation shown in Fig. 10(a)

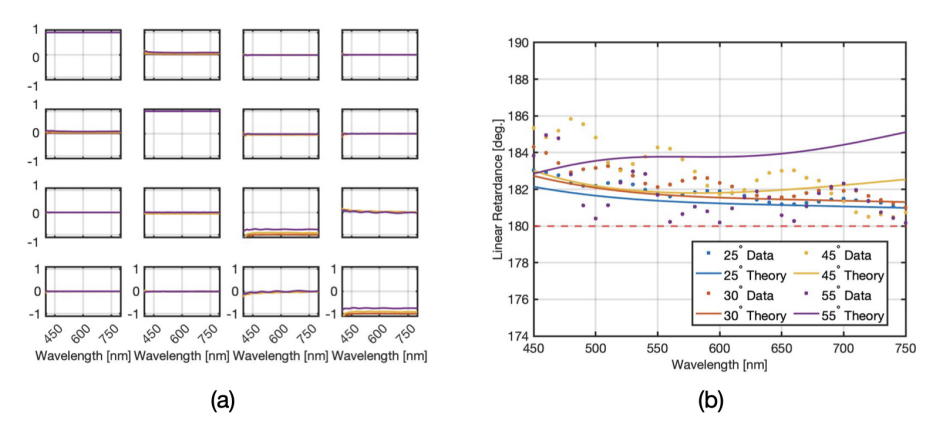


Fig. 13. Data with the same AOI is plotted with same color across both figures. (a) Measured Mueller matrix data at 25, 30, 45, and 55 degrees AOI are shown as a function of wavelength. The negative C-plate compensator does an excellent job of correcting the retardance polarization aberrations in aluminum. Diattenuation is not corrected, as an AR coated was not applied to the fabricated device. (b) Residual retardance for the simulated design is compared with measured values. The red dashed line represents the 180 degree geometric transformation due to reflection, or zero retardance. The fabricated device shows agreement with theory from 450nm to 700nm.

Figure 13(b) plots the theoretical residual retardance curves for the design as well as measured values at 25, 30, 45, and 55 degrees AOI, showing agreement with theory. The red dashed line at 180 degrees represents the retardance from an ideal reflection due to the geometric transformation from reflection at normal incidence. As the merit function references the ideal reflection in Eq. (11), 180 degree retardance is the non-polarizing, optimized value. Finally, we estimate the sensitivity of the dichroic compensator design and the aluminum coated mirror compensator design by performing a Monte Carlo simulation. In this calculation, the thickness and alignment of each layer are perturbed. The fabricated dichroic filter compensator had individual layers

which had retardance values very close to theory. The Monte Carlo simulation therefore only took into consideration the alignment between each of the layers. The design was perturbed 10,000 times with the alignment of each layer varied by up to ± 1 degree. The standard deviation in the resulting retardance is plotted in Fig. 14(a).

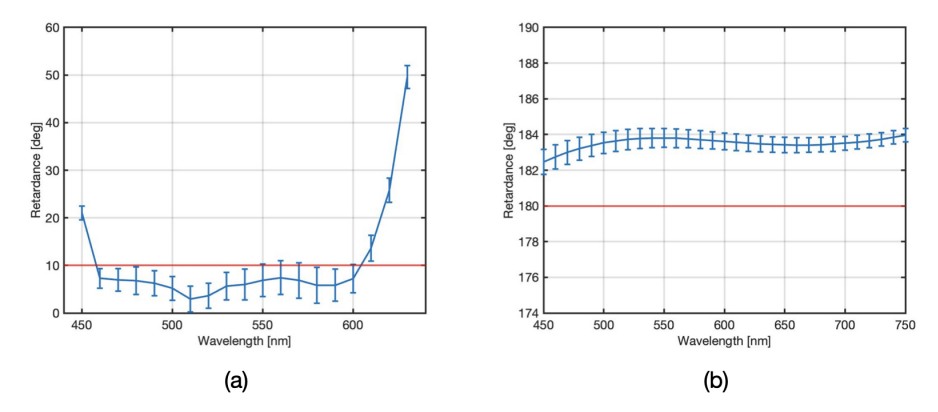


Fig. 14. Monte Carlo simulations with 10,000 runs are shown (a) Retardance as a function of wavelength is plotted with the standard deviation for the dichroic filter compensator for the case where the alignment between the layers is varied by ± 1 degree. The solid red line is the threshold of 10 degrees of residual retardance. (b) Retardance as a function of wavelength is plotted with the standard deviation for the aluminum compensator at a 55-degrees angle of incidence, for the case where the thickness of the negative C-plate layer is perturbed by $\pm 5\%$ of the design thickness. The red line represents the ideal 180-degree retardance due to geometric transformation.

Figure 14(b) shows the result of an additional Monte Carlo simulation with 10,000 runs. Here, the thickness of the negative C-plate layer on the aluminum compensator is varied by $\pm 5\%$ of the design thickness. The standard deviation of the resulting retardance at 55 degrees AOI is plotted along with the theoretical curve. Monte Carlo simulations of the aluminum compensator were performed at 55 degrees AOI, as the deviation from the ideal non-polarizing performance was the largest at 55 degrees. Tolerancing at the AOI with the largest deviation from the ideal gives the best indication of the stability of the design from fabrication imperfections. The red line represents the ideal 180 degree retardance from the geometric transformation of reflection. Our results show that variation of ± 1 degree in alignment can lead to approximately ± 5 degrees of retardance variation in the dichroic compensator design and that a variation of $\pm 5\%$ of thickness can lead to approximately a ± 1 degree of retardance variation in the aluminum coated mirror compensator design.

5. Conclusions

In this work, polarization aberration compensation devices for both dichroic spectral filters and metal-coated mirrors are presented. These devices correct for both diattenuation and retardance over a large spectral bandwidth. To demonstrate the utility of our method, we apply our technique to correct the retardance of a dichroic bandpass filter (Edmund Optics model #69-205). The Mueller matrix of the filter was measured as a function of wavelength, and the retardance was found to be over a quarter-wave at wavelengths longer than 600nm. A compensator utilizing multiple layers of birefringent nematic A-plate LCP was used to reduce the parasitic retardance. The compensator was fabricated and measured, showing correction of the parasitic retardance to below 10 degrees in the wavelength range of 470nm to 600nm, nearly the entire operating bandwidth of the spectral filter. In addition, we demonstrate the utility of our technique to

correction of polarization aberrations in an aluminum coated mirror. Reflections from the aluminum cause both diattenuation and retardance. A thin-film of negative C-plate LCP material was used to reduce the retardance, while a thin-film of fluoropolymer was optimized to reduce diattenuation of the device to no more than 5% from 450nm to 800nm over a 55-degree cone of angles. Further improvement of the design can include larger angular and spectral bandwidth, utilizing additional layers of birefringent films. Polarization aberration compensator devices such as these have applications in polarization sensitive interferometry, polarimetry, and displays, as well as in high contrast imaging such as astronomy.

Funding. National Science Foundation (1918260, 2053754).

Disclosures. Arizona Board of Regents on Behalf of the University of Arizona (P).

Data availability. Data underlying the results presented in this paper are not publicly available at this time but may be obtained from the authors upon reasonable request.

References

- 1. M. Mansuripur, Field, Force, Energy and Momentum in Classical Electrodynamics (Bentham, 2017).
- 2. H. A. Macleod, Thin-Film Optical Filters (CRC, 2017).
- 3. R. A. Chipman, W. T. Lam, and G. Young, Polarized Light and Optical Systems (CRC, 2019).
- 4. R. Chipman, "Polarimetry," in OSA Handbook of Optics, (McGraw-Hill, 2010).
- 5. G. P. Können, Polarized light in Nature (Cambridge University Press, 1985).
- G. P. P. L. Otten, F. Snik, M. A. Kenworthy, C. U. Keller, J. R. Males, K. M. Morzinski, L. M. Close, J. L. Codona, P. M. Hinz, K. J. Hornburg, L. L. Brickson, and M. J. Escuti, "On-sky performance analysis of the vector apodizing phase plate coronagraph on MagAO/CLIO2," The Astrophys. J. 834(2), 175 (2017).
- G. P. P. L. Otten, F. Snik, M. A. Kenworthy, M. N. Miskiewicz, and M. J. Escuti, "Performance characterization of a broadband vector apodizing phase plate coronagraph," Opt. Express 22(24), 30287–30314 (2014).
- J. B. Breckinridge, W. S. T. Lam, and R. A. Chipman, "Polarization aberrations in astronomical telescopes: The point spread function," Publ. Astron. Soc. Pac. 127(951), 445

 –468 (2015).
- 9. J. M. Davis, "Polarization aberrations in coronagraphs," Ph.D. thesis, University of Arizona (2019).
- 10. B. Daugherty, "Advances in polarization engineering," Ph.D. thesis, University of Arizona (2019).
- 11. D. Sabatke, J. S. Knight, and M. R. Bolcar, "Polarization ray tracing and polarization aberration compensation in reflective astronomical telescopes," in *Optical Modeling and Performance Predictions X*, vol. 10743 M. A. Kahan and M. B. Levine-West, eds., International Society for Optics and Photonics (SPIE, 2018), pp. 43–53.
- 12. Q. Hu, C. He, and M. J. Booth, "Arbitrary complex retarders using a sequence of spatial light modulators as the basis for adaptive polarisation compensation," J. Opt. 23(6), 065602 (2021).
- 13. J. Heath, M. Kupinski, E. Douglas, K. Hart, and J. Breckinridge, "Mueller matrix maps of dichroic filters reveal polarization aberrations," in *Space Telescopes and Instrumentation 2020: Optical, Infrared, and Millimeter Wave*, vol. 11443 M. Lystrup, M. D. Perrin, N. Batalha, N. Siegler, and E. C. Tong, eds., International Society for Optics and Photonics (SPIE, 2020), pp. 716–726.
- 14. Edmund Optics, "650nm, 25mm Diameter," Dichroic Shortpass Filter (2022). Datasheet.
- 15. J. M. Krijger, R. Snel, G. van Harten, J. H. H. Rietjens, and I. Aben, "Mirror contamination in space i: mirror modelling," Atmos. Meas. Tech. 7(10), 3387–3398 (2014).
- S. Miller, L. Jiang, and S. Pau, "Birefringent coating to remove polarization dependent phase shift," U.S. Patent Application 63/239184 (2021).
- 17. D. Yang and S. T. Wu, Fundamentals of Liquid Crystal Devices (John Wiley & Sons, 2010).
- 18. S.-T. Wu, "Birefringence dispersions of liquid crystals," Phys. Rev. A 33(2), 1270–1274 (1986).
- W. Swindell, "Handedness of polarization after metallic reflection of linearly polarized light," J. Opt. Soc. Am. 61(2), 212–215 (1971).
- S. Miller, L. Jiang, and S. Pau, "Polarization aberration compensation for reflective surfaces," U.S. Patent Application 63/269065 (2022).
- J. H. Hong, "Precision compensation for polarization anisotropies in metal reflectors," Opt. Eng. 43(6), 1276–1277 (2004).
- M. K. Yang, R. H. French, and E. W. Tokarsky, "Optical properties of Teflon® AF amorphous fluoropolymers," J. Micro/Nanolithogr., MEMS, MOEMS 7(3), 033010 (2008).
- S. Miller, L. Jiang, X. Tu, and S. Pau, "Patterned liquid crystal polymer c-plate retarder and color polarizer," Appl. Opt. 60(6), 1500–1507 (2021).
- V. Chigrinov, H. S. Kwok, H. Takada, and H. Takatsu, "Photo-aligning by azo-dyes: Physics and applications," Liq. Cryst. Today 14(4), 1–15 (2005).
- L. Jiang, S. Miller, X. Tu, M. Smith, Y. Zou, F. Reininger, and S. Pau, "Patterned achromatic elliptical polarizer for short-wave infrared imaging polarimetry," Opt. Express 30(2), 1249–1260 (2022).
- L. Li, S. Shi, and M. J. Escuti, "Improved saturation and wide-viewing angle color filters based on multi-twist retarders," Opt. Express 29(3), 4124–4138 (2021).

27. S. Y. Lu and R. A. Chipman, "Interpretation of mueller matrices based on polar decomposition," J. Opt. Soc. Am. A 13(5), 1106–1113 (1996).